Experimental and novel modeling evaluation of Nano-sized silicon carbide reinforced commercial casting aluminum alloy matrix

Kasinath Dasmohapatra, Debi Rasad Singh, Pradyut Kumar Swain, Bibhuti Bhusan Sabat

Department of Mechanical Engineering, NM Institute of Engineering and Technology,Bhubaneswar , Odisha
Department of Mechanical Engineering, Raajdhani Engineering College,Bhubaneswar,Odisha
Department of Mechanical Engineering,Aryan Institute of Engineering and Technology Bhubnaeswar , Odisha
Department of Mechanical Engineering,Capital Engineering College,Bhubaneswar,Odisha

ABSTRACT: *Experimental and modeling investigations were carried out on the porosity, wear, hardness, elongation, yield strength and ultimate tensile strength (UTS) of these nano-composites. The density measurements showed that the amount of porosity in the composites increased with increasing the volume fraction of nano-particles. In the current research, nano-composites of commercial casting aluminum alloy reinforced with nano-silicon carbide were produced. The wear sliding test revealed that composites offer superior wear resistance as compared to the alloy irrespective of nano-particles volume fraction. The tensile strength results show that the yield strength and ultimate tensile strength of the composites increased with increasing volume fraction of nano-particles. The incorporation of nano-particles deteriorates the ductility of A356 alloy. However, the elongation remains rather constant with increasing the volume fraction of nano-particles. In the other word, increasing the nano-sized ceramic particles content helps to strengthen the composites, while the ductility is retained. In this paper, a technique based on artificial neural network (ANN) and finite element method (FEM) was proposed to investigate on nano-silicon carbide reinforced commercial casting aluminum alloy matrix. It was observed that prediction of this study is consistent with experimental measurements for aluminum matrix composites.*
Keywords: Nano composites, FEM, Silcon carbide

I. INTRODUCTION

The increasing demand for weight reduction and low fuel consumption in the structural applications, particularly aerospace and automotive industries has had a marked effect on the judicious selection of materials. There has been a great upsurge in using aluminum alloys, owing to their low density, high thermal conductivity and high specific strength, which leads to the weight reduction resulting in a consider-able economic advantage [1–3].

However, their low hardness and poor wear resistance are the main obstacles for their high performance mechanical and tribologi-cal applications. To overcome this problem, hard reinforcement phases such as particulates, fibers, and whiskers are introduced into Al-based matrix in order to improve their high specific strength, stiff-ness, wear resistance, fatigue resistance and elevated temperature applications [4–10].

Particulate Aluminum Matrix Composites (AMCs) are isotropic in their properties and are easier to process via powder metallurgy or cast ranging route compared to AMCs reinforced with ceramic whiskers and fibers.

There are several manufacturing techniques for particle reinforced AMCs such as liquid metal infiltration, spray decomposition, squeeze casting, compocasting, powder metallurgy and mechanical alloying [11–13]. Stir casting of MMCs is an attractive processing method for these advanced materials since it is relatively inexpensive, and offers a wide variety of material and processing condition options. General-ly, these composites consist of a metal matrix, which is melted during casting, and ceramic reinforcement which is added to the molten ma-trix material by a mechanical stirrer [14].

The enhancement in tribological properties of AMCs has been ef-fectively attainable by introducing the ceramic particles. It has been generally observed that increasing the SiC or Al_2O_3 particle content enhances the wear resistance of the base alloy. The wear resistance of the composite was found to be considerably higher than that of the matrix alloy and increased with increasing particle content. The hard particles resist against destruction action of abrasive and pro-tect the surface, so with increasing its content, the wear resistance enhances. This result is consistent with the rule that in general, mate-rials with higher hardness have better wear and abrasive resistance [15–17].

Numerous research works have been reported on mechanical properties and dry sliding wear behavior of AMCs reinforced with various particulates such as SiC, boron, TiC, Si_3N_4, silica sand, MgO, B_4N and Al_2O_3. Reinforcement of aluminum alloys with Al_2O_3 or SiC has generally been observed to improve the ultimate

tensile and the yield strengths of the metal. However, the ductility of the AMCs deteriorates significantly with high ceramic particle concentration. In order to retain the ductility, it will be attractive to produce as-cast lightweight bulk components of metal matrix nano-composites (MMNCs) with uniform reinforcement distribution and structural integrity [18–22].
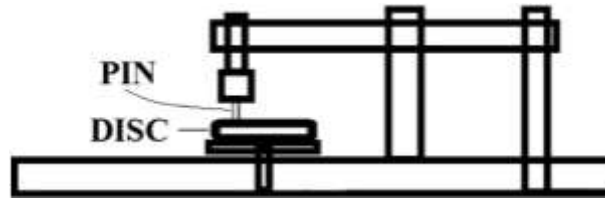

Fig. 1. Schematic representation of the neural network architecture.

Recent investigation found that the addition of a mere 1.5 vol.% nano-Al_2O_3 particulates to Al and Mg alloys was able to yield mechan-ical properties that were comparable and even superior to those of high strength Al and Mg composites containing a much higher level of micro sized ceramic particles.

Previous works on Al-based composites reinforced with ceramic particulate had reported that the fine sized particle was able to suppress the occurrence of delamination wear in sliding against stain-less steel. Al-based metal matrix composites are prone to suffer wear by delamination. Since the discontinuity at the interface be-tween the reinforcement and matrix promote crack nucleation and propagation which are central to mechanic of delamination. This mechanism often leads to wear rate comparable or even higher than those seen in unreinforced alloy. It is expected that the use of low levels of nano-sized reinforcement in AMCs would appear to address these earlier problems [19,22].

The artificial neural networks were first introduced by McCulloch et al., who suggested that the biological function of the human brain could be emulated by a simplified computational model. The theory of artificial neural networks (ANNs) remained out of interest for a long time. However, during the last three decades a huge growth in this research field has been reported and several ANN architectures have already proved their efficiency in diverse aspects. ANNs are suitable for simulating physical phenomena such as processing– structure–properties relations since the phenomena are characterized by multiple inputs and have nonlinear and complex relationships be-tween the input and output variables. The structure or architecture of ANNs is usually specified by the number of the layers in the ANN model and the number of the neurons in each layer [23–31]. As shown in Fig. 1, the general structure of the implemented ANN models consists of an input layer, a hidden layer and an output layer.

It is extremely challenging for the conventional mechanical stir-ring method to distribute and disperse nano-scale particles uniform-ly in metal melts because of the poor wettability and higher specific surface areas of nanoparticles which lead to agglomeration and clustering.

In this paper, the mechanical properties and sliding wear proper-ties of A356 composite reinforced with nano-SiC particulates were first experimentally investigated and then the combination of FEM with ANN is implemented for modeling of these properties.
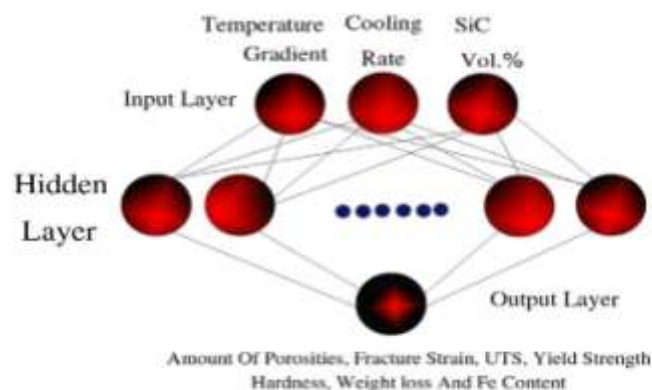

Fig. 2. Schematic diagram of the abrasion wear test.

II. EXPERIMENTAL

Casting Al–Si matrix composites reinforced with the nano-SiC particles have been used for the present study. The Al–Si alloy has the chemical composition of 7.5% Si, 0.38% Mg, 0.02% Zn, 0.001% Cu, 0.106% Fe, and the rest Al. This alloy has been selected because of its good fluidity as well as the presence of silicon and magnesium. A mixture of nano-SiC and aluminum particles with respectively aver-age particle size of 50 nm and 16 μm was used as the reinforcement. The required amount of SiC was calculated according to the ratio of Al/SiC. The preparation of the this mixture is described in previous work [19]. The addition of 1 wt.% magnesium to the melt promote wetting by reducing the surface tension of the melt, decreasing the solid–liquid interfacial energy of the melt, or inducing wettability by chemical reaction.

The process involved melting the alloy in the graphite crucible using an electrical resistance furnace. The furnace is controlled using a J-type thermocouple located inside the gas chamber. The temperature of the alloy was raised to about 750 °C and stirred by a graphite impeller. The powder mixture was inserted into an alumi-num foil by forming a packet. The packets were added into molten metal of crucible when the vortex was formed. The packet of mixture melted and the particles started to distribute around the alloy sam-ple. It was stirred for 15 min at approximately 600 rpm speed and then composite slurry was step cast into the CO_2-sand mold.

There is a nitrogen supply to the crucible in order to minimize the oxidation of molten aluminum.

The experimental density of the composites was obtained by the Archimedian method of weighing small pieces cut from the compos-ite cylinder first in air and then in water, while the theoretical density was calculated using the mixture rule according to the weight frac-tion of the particles. The amount of porosity in the cast alloy and the composite was determined by comparing the measured density with that of their theoretical density.
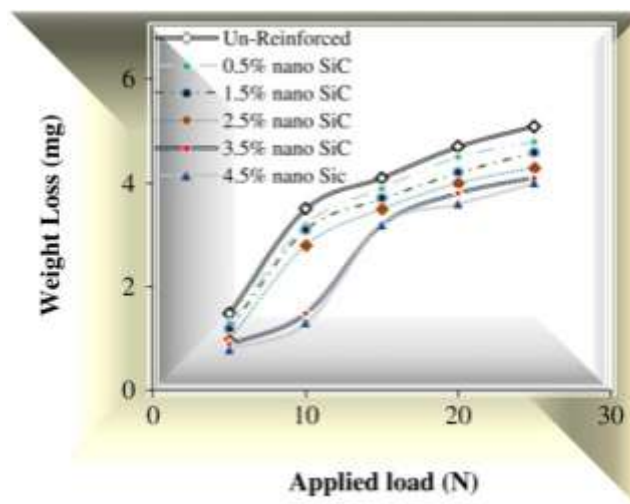

Fig. 3. Effect of applied load on wear resistance.

The tension tests were used to assess the mechanical behavior of the composites. The tensile specimens were machined from compos-ite rods according to ASTM.B 557 standard. For each volume fraction of SiC particles, three samples were tested. To study the hardness, the Brinell hardness values of the samples were measured on the polished samples using a ball with 2.5 mm diameter at a load of 31.25 kg.

Sliding wear tests were conducted in pin-on-disk wear testing apparatus under varying applied loads against case hardened steel disk of hardness 63 HRC. Test specimens were cut and shaped in the form of pins having 6 mm in diameter and 25 mm in height. Before the abrasion tests, each specimen was polished to 0.5 μm. The pin samples were solution treated at 540 °C for 4 h, quenched into warm water (40 °C) and then peak aged to T6 condition (155 °C for 9 h). Fig. 2 shows Schematic diagram of the abrasion wear test. The experiment was carried out at room temperature (21 °C, relative humidity 55%) with water as the lubricant. The samples were cleaned with acetone and weighed (up to an accuracy of 0.01 mg using microbalance) prior to and after each test. The temperature rise was recorded from the digital display interfaced with the wear test machine. A set of three samples was tested in every experimental condition, and the average along with standard deviation for each set of three tests is measured. The wear tests were conducted up to the total sliding distance of 2000 m.

III. FEM

The finite element method is a powerful technique for solving dif-ferential or partial differential equations as well as integral equations. For each triangular element, a linear relationship between nodes tem-peratures is used in the solution to the heat transfer problem. Eq. (1) is the general heat conduction equation, including unsteady heat storage and variable conductivity [23–30]:

If q is heat generation, ρ density, C heat capacity, L latent heat, k heat diffusion coefficient and k_0 solute partition coefficient. In this re-search, mechanical properties are considered to be related to cooling rate, temperature gradient and volume percentage of nano-SiC. The FEM method is used for discretization and to calculate the transient temperature field of quenching.

3.1. Neural networks

Artificial neural networks have been used widely in many applica-tion areas. In the most of the applications a Multilayer Perceptron (MLP) with the back-propagation (BP) training algorithm is used. MLP is defined by its architecture that includes processing elements (PE), their interconnections, and its activation function. MLP basically implements function f that maps a set of given input values.

The wear rate of the unreinforced alloy is found to be higher than that of the composites. This is primarily due to the fact that the hard dispersoids, present on the surface of the com-posite, act as protrusions, protect the matrix from severe contact with the counter surfaces [4–6], and thus resulting in less wear in composite as compared to that in the alloy. The hard particles resist against destruction action of abrasive and protect the surface, so with increasing its content, the wear resistance enhances. Addition-ally, the hard dispersoid makes the matrix alloy plastically con-strained and improves the high temperature strength of the virgin alloy.

It calculates the network output, the error vectors, and the Jacobi-an matrix for each pattern. Then, it computes w using Eq. (7) and recalculates the error with w + w as network weights. If the error has decreased, μ is divided by β, the new weights are maintained, and the process starts again; otherwise, μ is multiplied by β, w is cal-culated with a new value, and it iterates again [31–34].

It may be noted in Fig. 3 that the wear rate in all the samples increases marginally with applied load prior to reaching the critical load. The effec-tive wear from the specimen surface is due to the combined effect of a number of factors. The increase in the applied load leads to increase in the penetration of hard asperities of the counter surface to the softer pin surface, increase in micro cracking tendency of the subsurface and also increase in the deformation and fracture of asperities of the softer surface. On the other hand, higher amount of material from the pin sur-face gets accumulated at the valleys between the asperities of counter surfaces resulting in reduction in height and cutting efficiency of counter surface asperities. Beyond the critical load for each composite, the wear rate starts increasing abruptly with the applied load.

$$y : y ¼ f ðx Þ \qquad (i)$$

MLP tries to find the best possible approximation of the function f as a complex combination of elementary nonlinear functions. This approximation is coded in the neurons of the network using weights that are associated with each neuron. The weights of MLP are learned using an iterative procedure in which examples of correct input– output associations are shown to the network. The weights are mod-ified when the network starts to mimic the desirable input–output behavior. This ability to learn from examples and the ability for gen-eralization to new situations are the most attractive features of the ANN paradigm.

The Levenberg–Marquardt algorithm (LM) is an approximation to the Newton method used also for training ANNs. The Newton method approximates the error of the network with a second order expres-sion, which contrasts to the back-propagation algorithm that does it with a first order expression [25–32]. LM is popular in the ANN do-main (even if it is considered the first approach for an unseen MLP training task), although it is not that popular in the metaheuristics field. LM updates the ANN weights as follows:

$$w ¼ -{}^h\mu I þ \sum\nolimits^p_{p¼1} J^p ðwÞ^T J^p ðwÞ^{i-1} \nabla E ðwÞ \qquad (ii)$$

where J^p (w) is the Jacobian matrix of the error vector E^p (w) evalu-ated in w, and I is the identity matrix. The vector error E^p (w) is the error of the network for pattern p:

$$E^p ðwÞ ¼ T^p − O^p ðwÞ: \qquad (iii)$$

The parameter μ is increased or decreased at each step. If the error is reduced, then μ is divided by a factor β, while it is multiplied by β in other case.

It calculates the network output, the error vectors, and the Jacobi-an matrix for each pattern. Then, it computes w using Eq. (7) and recalculates the error with w + w as network weights. If the error has decreased, μ

is divided by β, the new weights are maintained, and the process starts again; otherwise, μis multiplied by β, w is cal-culated with a new value, and it iterates again [31–34].
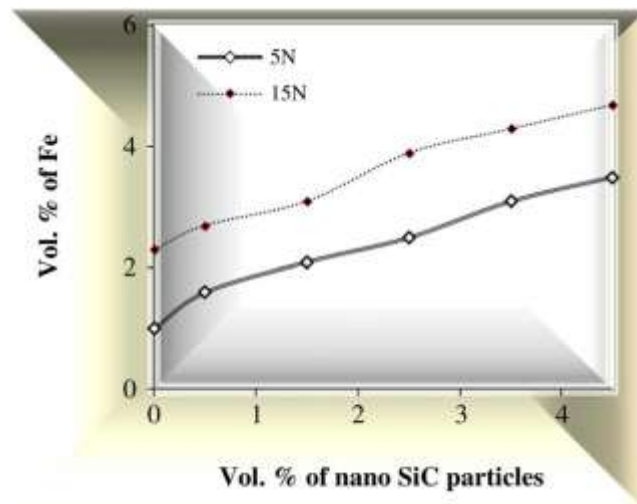

Fig. 4. Variations of the Fe content on the worn surface.

where A and F represent the actual and forecasting values respectively and N is the number of forecasting points.

IV. RESULTS AND DISCUSSION

The weight loss of the samples as a function of applied load is depicted in Fig. 3. The wear rate of the unreinforced alloy is found to be higher than that of the composites. This is primarily due to the fact that the hard dispersoids, present on the surface of the com-posite, act as protrusions, protect the matrix from severe contact with the counter surfaces [4–6], and thus resulting in less wear in composite as compared to that in the alloy. The hard particles resist against destruction action of abrasive and protect the surface, so with increasing its content, the wear resistance enhances. Addition-ally, the hard dispersoid makes the matrix alloy plastically con-strained and improves the high temperature strength of the virgin alloy [4–6]. During dry sliding wear of aluminum based composite, wear of the counterface is usually evident. The extent of iron deposi-tion is reported to be more significant for MMC/steel sliding couples in comparison to Al/steel sliding couples due to micro cutting and plowing of reinforcing hard ceramic particles on the counterface (Fig. 4). It is suggested that an extensive mechanical mixing took place between the aluminum matrix composite and the steel coun-terpart during sliding wear, and mechanically mixed layer (MML) containing elements from the two sliding counterparts were formed on the worn surface [35].

It may be noted in Fig. 3 that the wear rate in all the samples increases marginally with applied load prior to reaching the critical load. The effec-tive wear from the specimen surface is due to the combined effect of a number of factors. The increase in the applied load leads to increase in the penetration of hard asperities of the counter surface to the softer pin surface, increase in micro cracking tendency of the subsurface and also increase in the deformation and fracture of asperities of the softer surface. On the other hand, higher amount of material from the pin sur-face gets accumulated at the valleys between the asperities of counter surfaces resulting in reduction in height and cutting efficiency of counter surface asperities. Beyond the critical load for each composite, the wear rate starts increasing abruptly with the applied load. The load at which wear rate increases suddenly to a very high value is termed as the tran-sition load [36]. When the applied load is greater than the transition load, the wear rate of the composite shoots up to significantly higher value. This is attributed to the significantly higher frictional heating and thus the localized adhesion of the pin surface with the counter surface and also to the increase in softening of the surface material and thus more penetration of the asperities. Under such conditions the material remov-al due to the delamination of adhered areas, micro cutting and micro fracturing increases significantly. This leads to destruction of MML, which was formed at lower applied load at the initial period of sliding. As a result, after a critical load there is a transition from smooth linear in-crease wear rate to sudden increase in wear rate. It was reported in the previous research that when the applied load induces stresses that ex-ceed the fracture strength of carbide particles, the particles fracture and largely lose their effectiveness as load bearing components. The shear strains are transmitted to the matrix alloy and wear

proceeds by a subsurface delamination process [36]. Furthermore, liberated reinfor-cing particles as wear debris roll over the contacting surfaces which cre-ate three body abrasion type situations and causing more wear on both the contacting surface. However, extent of this situation depends on slid-ing speed, applied load and frictional heating. In this case, the lower duc-tility of Al–SiC composites appears to control the wear rates rather than the hardness of particles, resulting in wear rates almost similar to those observed in Al alloys without SiC reinforcement. On the other hand, when the nominal load induces stresses lower than the strength of par-ticles the particles act as load bearing components. In this case, the SiC particles remain intact during wear in order to support the applied load and act as effective abrasive elements. The particles protruding from the surface of the composite bear most of the wear load, and the surface hardness of the composite is mainly a result of the hardness of the particles [26–29].
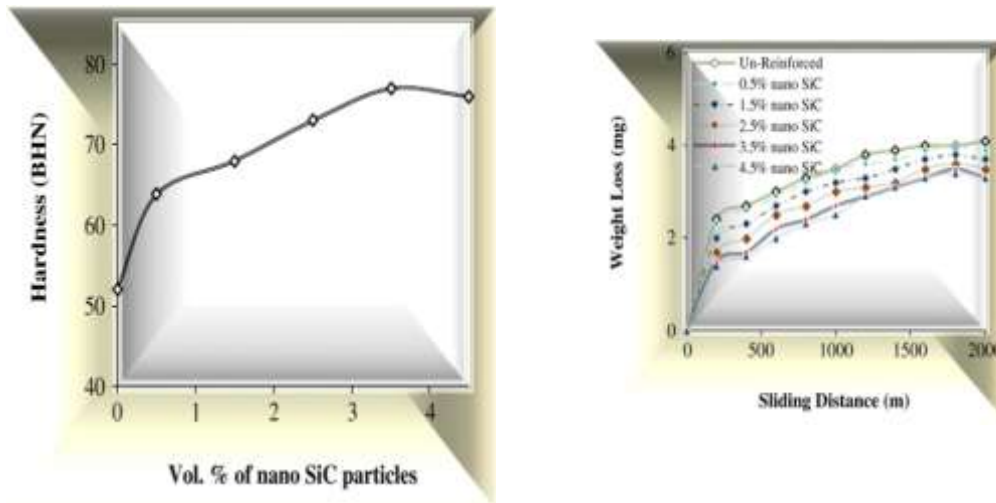

Fig. 5. Weight loss as a function of sliding distance.   Fig. 6. Hardness as a function of nano-SiC particles volume fraction.

Sliding wear is related to asperity-to-asperity contact of the two counter surfaces, which are in relative motion against each other. Fig. 5 shows the weight loss as a function of sliding distance at an applied load of 15 N. It is noted that the weight loss of the compos-ites is less than that of unreinforced alloy, increases with increase in sliding distance, and has a declining trend with increasing the particles volume fraction.

In general, composites offer superior wear as compared to the alloy irrespective of applied load and sliding speed [36]. This result is consistent with the rule that in general, materials with higher hard-ness have better wear and abrasive resistance (Fig. 6). The higher hardness of the composites could be attributed to the fact that SiC particles act as obstacles to the motion of dislocation [37,38].

At the initial stage of sliding, the wear is mainly due to fragmenta-tion of asperities and removal of material due to cutting and flowing actions of penetrated hard asperities into the softer surface. Higher amount of stress is expected to act on the asperities, due to the great-er degree of their hardness and sharpness. Because of the higher stress concentration on these points, they get plastically deformed and some of the sharpest asperities get fractured due to combined ac-tion of normal and shear stress. During the sliding, in fact a consider-able fraction of energy is spent on overcoming the frictional force, which leads to heating of the contact surfaces. Thus, it is expected that initially the temperature of the contact surface is less and hence the asperities are expected to be stronger and more rigid. As time progresses, the frictional heating increases, which leads to higher temperature and softening of the surface materials.

Fig. 7 represents the variation of temperature with sliding distance at an applied load of 20 N. It is noted that temperature rise is greater in the case of unreinforced alloy as compared to that in the composite irrespective of the applied load and surface conditions. In general, it is observed that the temperature initially increases at a sharp rate and then gradually reaches to a stable value. The rise in surfaces temper-ature is an outcome of a couple of facts that cause heating of the con-tact surfaces. During sliding, frictional force acts between the counter surfaces, which caused frictional heating of them. While the counter surfaces are in relative motion, the frictional heating is continuous be-cause of insufficient time for heat dissipation. Initially, the asperities are stronger and sharper, and that is why frictional force and as a re-sult frictional heating takes place at higher rate. After a certain period, because of the increase in flowability of the material on the specimen surface, slipping action is higher which results in reduction of fric-tional heating. The more possibility of

adhesion between the counter surfaces leads to higher degree of friction. Because of these counter phenomena, frictional heating remains almost constant as observed in Fig. 7. It is also mentioned earlier that surface and subsurface defor-mation took place during sliding which also causes heating of the contact surfaces.

Because of combined action of load, sliding speed and sliding dis-tance, subsurface micro cracks are generated which finally leads to re-moval of wear debris, especially from asperity contacts. In addition higher temperature rise also leads to greater flowability of surface materials and thus increases greatly the possibility of compaction of wear debris on the specimen surface. In this case, valleys between the asperities of the counter surface gets partially occupied with the material of the specimen, which results in the reduction of surface abrasive action effectiveness of the counter surface asperities. With further increase in sliding distance, the temperature increases to a critical value at which specimen surface gets oxidized. This oxidized surface either gets fragmented or becomes stable to some extent. The fragmented oxide particles sometimes act as lubricating agent and thus these oxide layers reduce the effective wear rate. Further-more, the fragmentation and compaction of wear debris, counter sur-face material and thin oxide layers leads to formation of mechanically mixed layer which protects the specimen surface from wear [36]. However, further increasing sliding distance leads to increasing tem-perature which leads to subsurface softening and because of plastic incompatibility, and thermal mismatch, the MML gets fractured and subsequently removed from the specimen surface. Thus at higher sliding distance it is expected that the formation and removal of MML are taking place simultaneously and the rate of removal and the rate of growth of MML might be same and thus the wear rate re-mains unchanged with sliding distance. It is reported that as the slid-ing distance reaches to the point of seizure, the MML becomes unstable because of greater degree of temperature rise in the subsur-face resulting in higher degree of thermal as well as plastic incompat-ibility between MML and subsurface [36,39].

Normally micron-sized particles are used to improve the ultimate tensile and the yield strengths of the metal. However, the ductility of the MMCs deteriorates significantly with high ceramic particle con-centration [40–43]. It is of interest to use nano-sized ceramic particles to strengthen the metal matrix, while maintaining good ductility [44]. Fig. 8 displays the tensile flow curves of the composites. It is noted that the addition of nano-particles deteriorate the ductility of A356 alloy. The stir casting method that is used in the present work to pro-duce the nano-composites can most probably create different inter-faces between nano-particles and matrices and thus, encourage crack initiation and propagation [9]. It is also noted that the
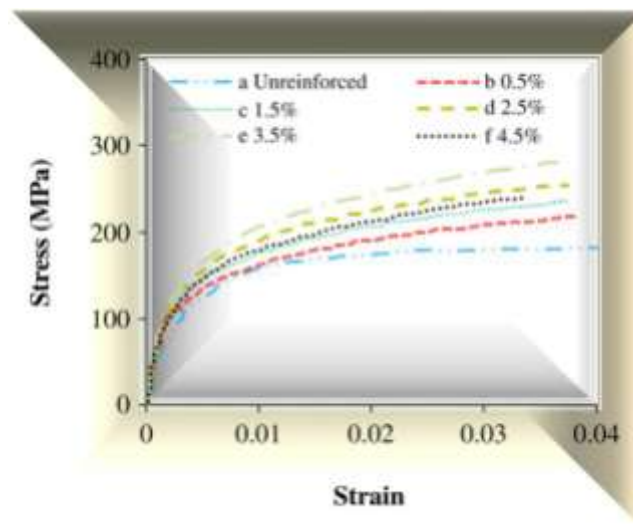

Fig. 7. Temperature as a function of sliding distance.
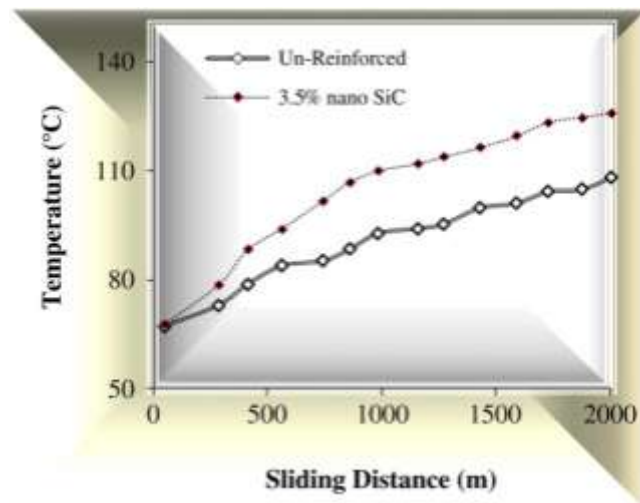
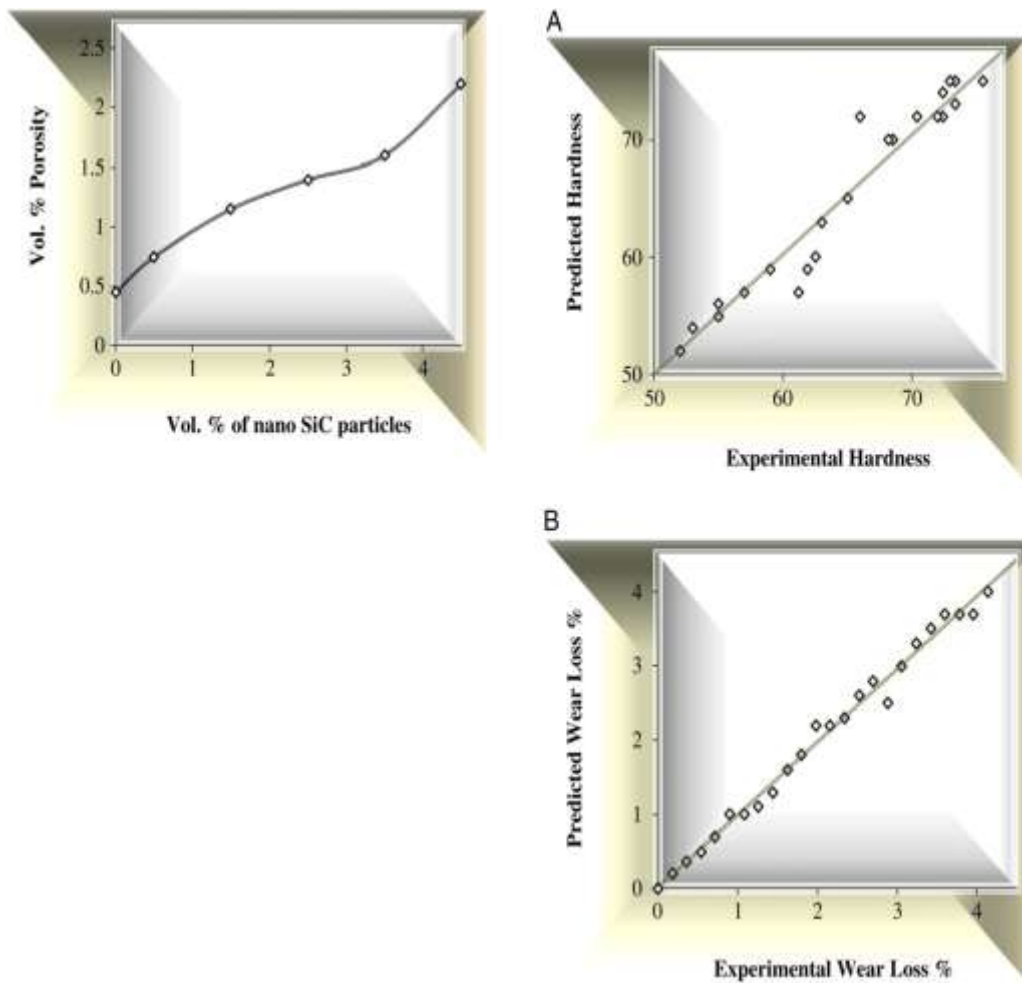**Fig. 8.** Flow curves in tensile deformation of the composites.

Fig. 9. Variations of porosity with the nano-SiC content.
Fig. 10. MAPE values for various neuron in the hidden layer.

elongation remains rather constant with the addition of nano-particles. This is consistent with the findings of Hassan and Gupta [45,46].

It could be observed that the flow curves do not show any sharp yield point irrespective of the material and the strength values in-creases with the addition of nano-SiC particles. The great enhance-ment in tensile flow stress observed in these composites is due to good distribution of the nano-SiC particles and low degree of porosity which leads to effective transfer of applied tensile load to the uni-formly distributed strong SiC particulates. The grain refinement and strong multidirectional thermal stress at the Al/SiC interface are also important factors, which play a significant role in the high strength of the composites. SiC particles have grain-refined strengthening ef-fect, since they act as the heterogeneous nucleation catalyst for alu-minum which is improved with increase in the volume fraction [47].

The difference between the coefficient of thermal expansion (CTE) values of matrix and ceramic particles generates thermally induced residual stresses and increase dislocations density upon rapid solidifi-cation during the fabrication process. The interaction of dislocations with the non-shearable nano-particles increases the strength level of composite samples. According to the Orowan mechanism, the nano-SiC particles act as obstacles to hinder the motion of disloca-tions near the particles in the matrix. This effect of particles on the matrix is enhanced gradually with the increase of particulate volume fraction [2,6].

According to the results of this experiment, quite significant improvement in strength is noted initially when particles are added; however, further increase in SiC content leads to reduction
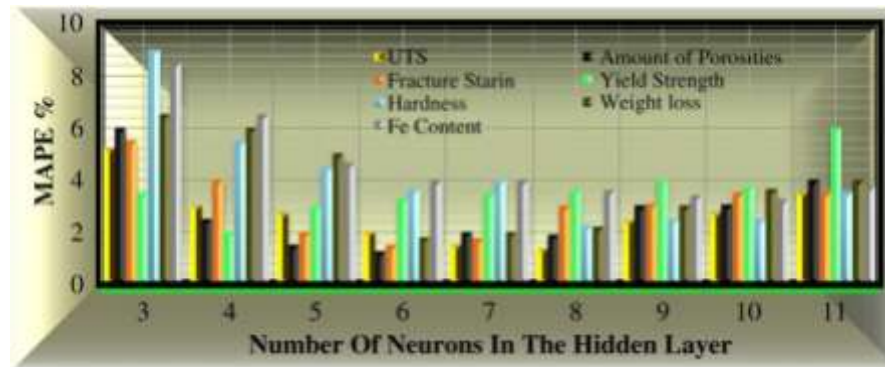

Fig. 11. Comparison between the experimental and predicted values: Hardness (a), Wear loss (b).

in strength values. The weakening factors of mechanical properties might be responsible for this including particles clusters and poros-ity (Fig. 9). Hereby, it is believed that strengthening and weakening factors of mechanical properties could neutralize the effect of each other and thus, the composite containing 3.5 vol.% SiC exhibits max-imum tensile flow stress.

Fig. **12**. Distribution of yield strength with 2% SiC in this model.

As shown in Fig. 1, the general structure of the implemented ANN models consists of an input layer, a hidden layer and an output layer.

The problem of choosing a suitable architecture for MLPs lies in specifying the activation function and the number of neurons in the hidden layer. Trial-and-error analysis resulted in the selection of a suitable activation function for each model. The selection of the number of hidden nodes in MLPs is both the most difficult and important step. Since the use of these training algorithms is indeed very time consuming process, it is important to be convinced that the obtained solutions are the optimum ones. Therefore, the error behavior of the neural network has to be observed to find the results with minimum errors. There is no known concept about selection of the number of neurons in the hidden layer. The neuron number in the hidden layer can be found experimentally. In Fig. 10, the mean absolute percentage error (MAPE) values are computed and given at the end of training process for various neurons in the hidden layer. The MAPE errors of the predictions for the entire data (train and test data) are:

UTS = 1.37 (with eight neurons in hidden layer)

Hardness = 2.25 (with eight neurons in hidden layer)

Amount of porosities = 1.25 (with six neurons in hidden layer)

Fracture strain = 1.5 (with six neurons in hidden layer)

Yield strength = 2.05 (with four neurons in hidden layer)

Fe content = 3.25 (with ten neurons in hidden layer)

Weight loss = 1.8 (with six neurons in hidden layer)

Therefore, a model was used with the mentioned properties. Random weightings are assigned to each processing element as an arbitrary starting point in the training process and the weightings are progressively altered on exposure to numerous repetitions of training examples. The model is verified against the cases in the test data file, which are independent of the cases in the train data file. Comparison between the experimental and predicted values of weight loss and hardness for A356 nano-composite at different cooling rate and temperature gradient is displayed in Fig. 11. The higher consistency of this model with experimental measurement can be easily observed. The remarkable agreement between the experimental and predicted values implies that the combination of FEM and ANN model can be used to predict the mechanical properties. In order to exhibit some results of A356 composite, the distribution of yield strength in this model is displayed in Fig. 12.

V. CONCLUSION

The wear resistance of the composite was found to be consider-ably higher than that of the matrix alloy and increased with increas-ing particle content. The hard particles resist against destruction action of abrasive and protect the surface, so with increasing its content, the wear resistance enhances. The higher hardness of the composite samples relative to that of the matrix Al-alloy could be at-tributed to the reducing grain size and existing of nano-hard particles acting as obstacles to the motion of dislocation. The addition of nano-particles resulted in significant improvements in yield strength and

UTS of the composites. Different strengthening mechanisms contrib-uted in the obtained strength improvements including Orowan strengthening, grain refinement, accommodation of CTE mismatch between the matrix and the particles, and the load bearing effects.

Unlike the experimental approach, which is time consuming, com-bination of FEM with ANN method is capable of generalizing the com-plex relationships and provide approximate solutions. Mechanical properties are related to cooling rate, temperature gradient and vol-ume percentage of SiC. Information obtained from the model predic-tions and simulations can be used as guidelines during the conceptual design and optimization of manufacturing processes thus reducing the time and costs that would otherwise be incurred by experimental methods.

REFERENCES
[1]   Y.T. Zhao, S.L. Zhang, G. Chen, X.N. Cheng, C.Q. Wang, Compos. Sci. Technol. 68 (2008) 1463–1470.
[2]   S.F. Hassan, M. Gupta, Metall. Mater. Trans. 36A (2005) 2253–2258.
[3]   M. Ostad Shabani, A. Mazahery, Int. J. Appl. Math Mech. 7 (2011) 89–97.

[4]   P.N. Bindumadhavan, T.K. Chia, M. Chandrasekaran, H.K. Wah, L.N. Lam, O. Prabhakar, Mater. Sci. Eng., A 315 (2001) 217–226.
[5]   S. Chung, B.H. Hwang, Tribol. Int. 27 (5) (1994) 307–314.
[6]   S.C. Lim, M. Gupta, L. Ren, J.K.M. Kwok, J. Mater. Process. Technol. 89/90 (1999) 591–596.
[7]   M. Roy, B. Venkataraman, V.V. Bhanuprasad, Y.R. Mahajan, G. Sundararajan, Metall. Trans. A 23 (1992) 2833–2846.
[8]   S. Skolianos, T.Z. Kattamis, Mater. Sci. Eng., A 163 (1993) 107–113.
[9]   M.K. Surappa, S.V. Prasad, P.K. Rohatgi, Wear 77 (1982) 295–302.

[10] M.O. Shabani, A. Mazahery, J. Mater. Sci. 46 (2011) 6700–6708.
[11] D.B. Miracle, S.L. Donaldson, Introduction to Composites, ASM Handbook, in: D.B. Miracle, S.L. Donaldson (Eds.), Composites, vol. 21, 2001, pp. 3–17, ASM International, Materials Park.
[12] T.W. Clyne, P.J. Withers, An Introduction to Metal Matrix Composites, in: Paperback Pub. in 1994 (Ed.), Cambridge University Press, Cambridge, 1993.
[13] T.W. Clyne, Metallic composite materials, in: R.W. Cahn, P. Haasen (Eds.), Physical Metallurgy, 4th ed., Elsevier, 1996, pp. 2568–2625.
[14] A. Mazahery, M.O. Shabani, Russ. Metall. (Metally) (2011) 699–707.
[15] P.N. Bindumadhavan, H.K. Wah, O. Prabhakar, Wear 248 (2001) 112–120.
[16] J.K.M. Kwok, S.C. Lim, Compos. Sci. Technol. 59 (1999) 55–65.
[17] S. Das, D.P. Mondal, G. Dixit, Metall. Mater. Trans. A 32 (2001) 633–642.
[18] H. Ferkel, B.L. Mordike, Mater. Sci. Eng., A 298 (2001) 193–199.
[19] A. Mazahery, M. Ostadshabani, J. Compos. Mater. 45 (2011) 2579–2586.
[20] K. Akio, O. Atsushi, K. Toshiro, T. Hiroyuki, J. Jpn. Inst. Light Met. 49 (1999) 149–154.
[21] J.R. Groza, Int. J. Powder Metall. 35 (1999) 59–66.
[22] M. Habibnejad-Korayema, R. Mahmudia, W.J. Pooleb, Mater. Sci. Eng., A 519 (2009) 198–203.
[23] M.O. Shabani, A. Mazahery, Appl. Math. Model. 35 (2011) 5707–5713.
[24] S.H. Mousavi Anijdan, A. Bahrami, H.R. Madaah Hosseini, A. Shafyei, Mater. Des. 27 (2006) 605–609.
[25] Y. Ko, H. Shang, Powder Technol. 205 (1–3) (2011) 250–262.
[26] L. Fratini, G. Buffa, D. Palmeri, Comput. Struct. 87 (2009) 1166–1174.
[27] R. Hamzaoui, M. Cherigui, S. Guessasm, O. ElKedim, N. Fenineche, Mater. Sci. Eng., B 163 (2009) 17–21.
[28] N.S. Reddy, A.K. Prasada Rao, M. Chakraborty, B.S. Murty, Mater. Sci. Eng., A 391 (2005) 131–140.
[29] F. Karimzadeh, A.A. Ebnonnasir, Foroughi, Mater. Sci. Eng. A 432 (2006) 184–190.
[30] K. Elsayed, C. Lacor, Powder Technol. 212 (1) (2011) 115–133.
[31] M.O. Shabani, A. Mazahery, M.R. Rahimipour, M. Razavi, J. King Saud Univ. Eng. Sci. (2011), doi:10.1016/j.jksues.2011.05.001.
[32] S.M. Tahir, A.K. Ariffin, M.S. Anuar, Powder Technol. 202 (2010) 162–170.
[33] Paulo J. Lisboa, F.G. Azzam, Neural Netw. 19 (2006) 408–415.
[34] A.M. Hassan, A. Alrashdan, T.M. Hayajneh, A.T. Mayyas, J. Mater. Process. Technol. 209 (2009) 894–899.
[35] K. Razavizadeh, T.S. Tyre, Wear 79 (1982) 325–333.
[36] M.O. Shabani, A. Mazahery, Synth. Met. 161 (2011) 1226–1231.

[37] P.S. Cooke, P.S. Werner, Mater. Sci. Eng., A 144 (1991) 189–193 15.
[38] D.P. Mondal, N.V. Ganesh, V.S. Muneshwar, Mater. Sci. Eng. 433 (2006) 18–31.
[39] S.C. Lim, M.F. Ashby, Acta Metall. 35 (1987) 1–24.
[40] R.G. Reddy, Rev. Adv. Mater. Sci. 5 (2003) 121.
[41] Y.C. Kang, S.L.I. Chen, Chem. Phys. 85 (2–3) (2004) 438–443.
[42] E.M. Maik, O. Beort, S. Kleiner, U. Vogt, Compos. Sci. Technol. 679 (11–12) (2007) 2377–2383.
[43] G. Wang, Z. Lu, C. Wang, Q. Ren, K. Zhang, Powder Technol. 214 (2) (2011) 188–193.
[44] K.M. Mussert, W.P. Vellinga, A. Bakker, S. Van Der Zwaag, J. Mater. Sci. 37 (2002) 789–794.
[45] S.F. Hassan, M. Gupta, J. Mater. Sci. 41 (2006) 2229–2236.
[46] S.F. Hassan, M. Gupta, Mater. Sci. Eng., A 392 (2005) 163–168.
[47] M.C. Watson, T.W. Cline, Acta Metall. Mater. 40 (1992) 135–140.